Modeling the shearing behavior of discontinuous rock mass incorporating dilation of joint aperture

Jintong Zhang[1], Mamoru Kikumoto[2], Hideaki Yasuhara[3], Sho Ogata[4], Kiyoshi Kishida[5*]

1 Department of Urban Management, Kyoto University, Kyoto, 615-8540, Japan

(zhang.jintong.38w@st.kyoto-u.ac.jp)

2 Department of Civil Engineering, Yokohama National University, Yokohama, 240-8501, Japan

(kikumoto-mamoru-fc@ynu.ac.jp)

3 Department of Civil and Environmental Engineering, Ehime University, Matsuyama, 790-8577, Japan

(hide@cee.ehime-u.ac.jp)

4 Department of Civil Engineering, Osaka University, Suita, 565-0871, Japan

(ogata@civil.eng.osaka-u.ac.jp)

5 Department of Urban Management, Kyoto University, Kyoto, 615-8540, Japan

(kishida.kiyoshi.3r@kyoto-u.ac.jp)

*Corresponding author: (kishida.kiyoshi.3r@kyoto-u.ac.jp)

Abstract

The shearing characteristics of rock joints govern the mechanical performance of discontinuous rock masses. The present study investigated the normal compression and shear behavior of rock joints through cyclic compression tests and direct shear tests. The irreversible relationship between the normal stress and the normal closure was confirmed by cyclic compression tests on rock joints. An elastoplastic model was proposed incorporating the aperture variation. A modified version of the critical state framework was developed for modeling the shearing and dilation behavior. Specifically, the initial state of the rock joints was determined according to the stress history. The proposed model for the mechanical behavior of rock joints was validated by predicting the experimental results. A parameter analysis was also performed to highlight the difference in the shear behavior of the rock joints due to the difference in the initial apertures.

Keywords: Discontinuous rock mass, shearing behavior, joint aperture, dilation, elastoplastic, critical state theory

1 Introduction

The mechanical performance of rock masses is an overwhelmingly important research topic for the design and construction of deep underground structures, such as geological repositories for nuclear waste, underground storage facilities for resources and geothermal production well for heat energy exploitation, because these projects have high safety standards and require long-term stability. Rock joints are critical constituents in discontinuous rock masses, and their properties often govern the mechanical behavior of the fracture materials. Therefore, incorporating the joint features and correctly predicting the shear behavior are of great significance for rock mass stability analyses.

The characteristics of rock joints have been investigated for developing constitutive laws, such as the Barton-Bandies model that considers joint roughness [1], a tangent formulation that considers the dislocated shear displacement [2], the JRC-JMC model that takes account of the matching condition [3], and the Grasselli-Egger model that is based on three-dimensional surface parameters [4]. Moreover, many theories have been applied to construct shear models. Contact theory models were formulated for modeling the shear behavior, which largely depends on the topography characteristics [5, 6]. Plasticity theory models, considering asperity degradation, have been established too [7, 8]. A constitutive model, considering the specific volume of soft rock, has also been developed based on the extended critical state theory [9]. The effect of joint planes on the strength and structure of soft rock has been investigated, and

one bounding surface plasticity model was proposed [10, 11]. However, the joint aperture has not been taken into account in the modeling of the shear behavior of discontinuous rock masses despite the sensitivity of the aperture to changes in the applied load and the great influence of the aperture on the shear behavior of rock joints. Thus, the incorporation of the aperture variation is necessary for modeling the shearing behavior of discontinuous rock masses.

The joint aperture, which depends upon the matching properties and surface geometry, controls the maximum deformation of the joints and the mechanical responses of discontinuous rock masses under the normal loading process. A closed joint (e.g., rock with an interlocked joint or well-matched joint) can only cause a slight movement of the joint walls. An open joint (e.g., rock with a mismatched joint or degraded asperities) allows for a considerable amount of normal displacement of the upper half of the specimen, as the joint tends to approach the complete state [3, 12, 13]. Simultaneously, the normal stiffness is substantially larger for a perfectly matched joint with a small joint aperture than an unmatched joint with a large joint aperture [3, 12, 14, 15]. In addition, the matched and unmatched types of rock joints with different apertures both demonstrated the plastic behavior of the initial loading cycles and the elastic behavior of the subsequent loading cycles in the extensive results obtained from cyclic compressive experiments [14–20]. Hence, based on the distinct effects and the variation in joint aperture, the evolution of each aperture under cyclic normal stress needs to be carefully considered.

63 The initial aperture response to the matching properties of the joint walls governs the peak
64 shear strength and dilation movement during the shear process. A smaller initial aperture usually
65 indicates that the rock joint has a mated interface. A higher peak shear stress is then required to
66 shave the contact asperities on the matched joint surfaces. In contrast, a larger initial aperture
67 indicates an unmated interface. The rock joint has relatively lower peak shear strength due to
68 the loosely interlocked asperities [3, 13, 15]. In addition, the change of joint aperture from the
69 interlocked state to the dislocated state is closely associated with the movement of dilation
70 during the shear process [21–24]. Moreover, an increase in the initial aperture caused by the
71 asperity degradation has been seen to decrease the dilation in multiple shear tests conducted on
72 the same rock joint [8, 13]. Similarly, the reduced initial porosity has been confirmed to increase
73 the volumetric strain in quartz material [25]. Therefore, the joint aperture is a vital and sensitive
74 parameter that influences and can be used to predict the shear and dilation behavior of rock
75 joints in the shear process.

76 The present study models the shear behavior of rock joints in conjunction with the dilation
77 of joint apertures. Cyclic loading and unloading tests were carried out to observe the aperture
78 variation of rock joints. The elastoplastic relationship between the normal stress and the relative
79 normal displacement was found to capture the rock joint aperture variation. A modified version
80 of the critical state framework [26, 27] was applied to delineate the rock joint's shearing and
81 dilation behavior in a unified manner. Moreover, the subloading surface concept [28] was

adopted to describe the plastic deformation before the critical state. The applicability of the model was validated by performing direct shear tests and comparing the results with those of the numerical modeling. Parameter analyses were conducted to discuss the effects of the initial apertures on the numerical response of the joint granite specimens.

2 Experimental evidence of compression and shear behavior of rock joint

Granite samples were analyzed to determine the mineral components, while the joint geometry was profiled to quantify the surface roughness. Then, multiple compression tests were carried out in three cycles of loading and unloading to observe the discontinuity's deformation and to calculate the rock joint's aperture. Direct shear tests were subsequently conducted under the constant normal loading condition to investigate the rock joint's shear and dilation behavior.

2.1 Material and methods

Granite specimens were sampled from a quarry located in the Inada district (specimens G1 and G2) and from a tunnel located in the Inagawa district (specimens G3 and G4), Japan. The mineral compositions of the granite specimens were determined by the X-ray diffraction (XRD) method. The Inada samples (G1 and G2) consisted of 56.75% quartz mineral, 42.00% feldspar mineral, and 1.25% biotite mineral. The Inagawa samples (G3 and G4) consisted of 30.10% quartz mineral, 33.67% feldspar mineral, and 36.23% biotite mineral. In addition, uniaxial compressive tests were conducted on intact granite to obtain the uniaxial compressive strength. Direct shear tests with different normal stress levels were conducted on rock with a flat joint

plane to obtain the frictional angle. The mechanical properties of the granite specimens are given in Table 1.

The joint granite specimens were prepared with a cross-section of 120 mm × 80 mm and a height of 120 mm. A single fracture was created along the center horizontal plane of each specimen. The profiled contour maps of the joint surfaces of one specimen (G1) are shown in Fig. 1 as an example. The specimen was placed in a shear box for vertical and horizontal loading tests. The compression and shear units were used to measure the load and displacement in the normal and shearing directions, respectively. An outline of the specimens and apparatus is given in Fig. 2.

For each specimen, the experimental procedure was repeated two times (two cases). Case-1 is the first experimental procedure. It included the surface profiling test and the enclosure of the specimen in the shear box, followed by the uniaxial compressive test and the direct shear test conducted on the specimen within the shear box. After the shear test in Case-1, the sheared rock was moved back to the original position and taken out of the shear box. The debris and gouge materials were removed, and the geometrical surfaces were profiled again. Then, the compression and shear tests were performed for Case-2. In the uniaxial compressive tests, the confining pressure was applied across the rock specimen from the initial loading stress to the final predetermined confining stress in the first loading process. Subsequently, the unloading process back to the initial stress condition was applied. The second and third loading and

118 unloading cycles were then performed successively under the same confining pressure process.
119 In the following direct shear tests, the corresponding constant normal pressure was loaded on
120 the specimen until reaching the residual state. During the shear process, the constant shear rate
121 of 0.1 mm/min was applied within the standardized shear rate of 0.02-0.2 mm/min (ISRM 1985).
122 The experimental conditions are shown in Table 2. The Joint Roughness Coefficient (*JRC*)
123 value of each joint interface was calculated by the backward analytical method of the Barton-
124 Bandies model [1] and are shown in Table 2.

2.2 Results of compression tests and shear tests

125 As one example, the compression test results of specimen G1 are plotted in Fig. 3. The
126 non-linear relationship between the normal stress-displacement in the two cases is given in Fig.
127 3 (a). After experiencing the compression and shear process in Case-1, the degradation of the
128 contact asperities caused the rough surfaces to flatten. Then, the poorly matching conditions
129 begin, and the normal displacement increases remarkably in the second compression process
130 (Case-2). An enlarged view of the process for Case-1 is shown in Fig. 3 (b). Large irreversible
131 displacement is observed in the first loading and unloading cycle. However, the permanent
132 closure seems to disappear during the second and third cycles, and the ensuing loading and
133 unloading process almost follows the same path. The discrepancy in the normal displacement
134 between the first loading path and the latter unloading/reloading paths is attributed to the stress
135 history. Here, the permanent closure in the initial loading process is referred to as irrecoverable

136 deformation. Simultaneously, the deformation of the normal displacement in the latter process
137 is regarded as recoverable behavior.

138 As the normal deformation is dependent on the stress history, the maximum closure was
139 measured in the third unloading path. As mentioned in the previous study, the compression
140 behavior can be approximately described by a hyperbolic function [15, 29]. In our study, Fig. 4
141 shows that the third unloading path of Case-1 for specimen G1 can be approximately fitted as
142 a hyperbolic curve. With the increase in normal stress, the path approaches a vertical line
143 asymptotically. The vertical asymptote represents the maximum normal displacement or the
144 maximum joint closure, which means the joint surfaces have been tightly matched under higher
145 normal stress. The hyperbolic closure model of Bandies [1] was applied to characterize the
146 relationship of the normal stress–displacement of the rock joint. This hyperbolic function is
147 given in Eq. (1).

148 $$\sigma_n = \frac{v_j k_n V_{mc}}{V_{mc} - v_j} \tag{1}$$

149 where σ_n, v_j, k_n, and V_{mc} are the normal stress, the normal closure, the normal stiffness of
150 the discontinuous rock mass, and the maximum closure of the joint aperture, respectively.

151 The joint aperture is defined as the mean distance between the adjacent joint surfaces. In
152 the third unloading path of the compression test, the current joint aperture is calculated by
153 subtracting the normal closure from the maximum joint closure as shown in Fig. 4. According
154 to the fitted hyperbolic curves, the initial aperture in the shear process was regarded as the

155 current aperture under the corresponding confining stress. The obtained initial apertures in the
156 first process (Case-1) and second shear process (Case-2) are given in Table 2. Comparing the
157 initial apertures and *JRC* values in the two cases of the four joint specimens, the results show
158 that the *JRC* value decreased and the initial aperture expanded after the shear test. After
159 undergoing the crushing of the asperities in the shear process, the decrease in the *JRC* values
160 indicates that the rougher surfaces are shaved to be smooth. Simultaneously, the increase in the
161 initial apertures indicates that the originally tightly matched condition of the adjacent surfaces
162 is declined to the later loosely matched condition. Hence, the expansion of the void space
163 between the lower and upper surfaces is induced. Consequently, applying the same normal
164 stress on the same specimen, enlarged initial apertures occur at the beginning of the second
165 shear process.

166 The shear stress-shear displacement relationship and the dilation curves of the first shear
167 and second shear tests on the four specimens are shown in Fig. 5. The apparent peak stress and
168 remarkable softening behavior were observed in the first shear process of Case-1. However, the
169 second shear process of Case-2 only shows the hardening behavior and not the salient peak
170 shear strength, except for in the case of specimen G2. During the shear process, the dilation is
171 assumed to equal the relative normal displacement of the upper half of the specimen. The
172 dilation increases with the shear displacement in both the first and second shear experiments.
173 Comparing the shear stress and dilation of the two shear cases, incorporating the initial aperture

174 given in Table 2, the rock joint with a small initial aperture in the first shear process exhibits
175 higher frictional resistance and larger dilation than the rock joint with a large initial aperture in
176 the second shear process. Therefore, the discrepancy of the shear behavior due to the difference
177 in the initial aperture must be considered in developing a model for rock joints.

3 Elastoplastic model for rock joint considering aperture variation

178 The aperture variation during the compression process can be obtained according to the
179 fitted hyperbolic curve and asymptote. The relationship between the joint aperture and normal
180 stress can be reconstituted as a straight virgin compression line and a set of straight loading and
181 unloading lines in a semi-logarithmic plot of normal stress and aperture. Fig. 6 shows the
182 variation of aperture during the cyclic loading and unloading tests of Case-1 for specimen G-1.
183 Here, a permanent change of the aperture was observed in the first loading path; and thus,
184 the variation in joint aperture in the first loading process was regarded as irreversible. The
185 aperture variations in the first unloading path, second loading/unloading paths, and third
186 loading/unloading paths were similar. The aperture variations in these paths are referred to as
187 reversible. The aperture variation of the rock joint from irreversible to reversible behavior is
188 similar to the volumetric transition of soil from the normal consolidation line to the swelling
189 line. The previous study indicated that the crushing of the rock joint's asperity contributes to
190 irreversible fracture deformation, whereas elastic deformation contributes to reversible
191 deformation [20]. Therefore, a hypothesis was conceived whereby the rock joint possesses a

192 transition from elastoplastic to elastic behavior in the first and latter compression processes.
193 Based on this hypothesis, an elastoplastic model incorporating the aperture variation was
194 introduced for modeling the shear behavior. The repeated loading and unloading process can be
195 simplified by the typical deformation behavior of the first cycle in the rock joint, as exhibited
196 in Fig. 7.

197 It is assumed that the incremental total relative displacement of the rock joint
198 $d\boldsymbol{\delta}\left(=\begin{pmatrix}d\delta_n\\ d\delta_s\end{pmatrix}\right)$, can be decomposed into elastic component $d\boldsymbol{\delta}^e\left(=\begin{pmatrix}d\delta_n^e\\ d\delta_s^e\end{pmatrix}\right)$ and plastic
199 component $d\boldsymbol{\delta}^p\left(=\begin{pmatrix}d\delta_n^p\\ d\delta_s^p\end{pmatrix}\right)$. Superscripts *e* and *p* denote the elastic and plastic parts of the
200 deformation, respectively, and subscripts *n* and *s* denote normal and shear components,
201 respectively.

202 $$d\boldsymbol{\delta} = d\boldsymbol{\delta}^e + d\boldsymbol{\delta}^p \tag{2}$$

3.1 Elastic stress–relative displacement relationship

203 According to the elastic behavior of the rock joint, shown in Fig. 7, the elastic stress-
204 relative normal displacement relationship is assumed as

205 $$\delta_n^e = \kappa ln\frac{\sigma_n}{\sigma_{n0}} \tag{3}$$

206 where κ is the unloading compression index, σ_n is the current normal stress, and σ_{n0} is the
207 initial normal stress where $\delta_n^e = 0$. Applying Taylor's expansion, Eq. (3) can be rewritten in
208 the following incremental form:

$$d\sigma_n = \underbrace{\frac{\sigma_n}{\kappa}}_{k_n} d\delta_n^e \tag{4}$$

where k_n is the normal stiffness dependent on the confining pressure, σ_n. Then, an elastic relationship is assumed as

$$d\boldsymbol{\sigma} = \underbrace{\begin{bmatrix} k_n & k_{ns} \\ 0 & k_s \end{bmatrix}}_{\boldsymbol{D^e}} d\boldsymbol{\delta^e} \tag{5}$$

where $d\boldsymbol{\sigma}\left(= \begin{pmatrix} d\sigma_n \\ d\sigma_s \end{pmatrix}\right)$ is the incremental traction vector, $\boldsymbol{D^e}$ is the elastic stiffness tensor, and k_s is the shear stiffness. For the dilatant joint, the joint normal stress depends on both the normal stiffness and the shear displacement [30]. Hence, k_{ns} is proposed to describe the stiffness controlling the effect of shearing on the confining stress. Two ratios, α and μ, are introduced to link shear stiffness with normal stiffness.

$$k_s = \mu k_n \tag{6}$$

$$k_{ns} = \alpha k_n \tag{7}$$

Moreover, the joint aperture variation, Δb, is considered to be equal to the relative normal displacement during the compression tests.

$$-\Delta b_n^e = \delta_n^e \tag{8}$$

Here, the compression direction is positive for the normal elastic displacement, δ_n^e.

3.2 Yield function considering the change in aperture

From the experimental evidence, the shear stiffness, shear strength, and dilation are primarily controlled by the aperture. A smaller aperture in a rock joint corresponds to larger

joint stiffness, shear strength, and dilation. A larger aperture in a rock joint results in smaller joint stiffness, shear strength, and dilation. The effects of the joint aperture on the above aspects are similar to the effects of the specific volume (void ratio) on soils/intact rocks. Moreover, an asymptotic critical state is reached at very large shear displacement. At the critical state, shear displacement increases without any further changes in the shear stress ratio and joint aperture. The shear stress ratio at the critical state is a unique, constant value specific to the rock joint. The joint aperture at the critical state is also a unique value given as a function of normal confining stress. These properties are likewise analogous to the critical state of soils and weak rocks. In the present study, the kernel concept assumes that

a) A unique critical state line in the space of confining pressure, shear stress, and aperture plays a central role in modeling a rock joint's behavior.

b) A rock joint's response is controlled by the difference of joint apertures between the current and the critical states. A joint having smaller apertures exhibits higher stiffness, strength, and dilation.

The procedure for developing the model is given below.

At a shear stress ratio, $\frac{\sigma_s}{\sigma_n}$, of zero, aperture b is assumed to stay on the first normal loading/compression line (*NCL*) or lower.

$$b \leq b_n - \lambda ln \frac{\sigma_n}{p_a} \tag{9}$$

Here, b_n is the joint aperture on the first normal loading line under atmospheric pressure. λ is the slope of the first normal loading line, and p_a (= 98 kPa) is the atmospheric pressure.

After applying large shear displacement, the rock joint eventually leads to the critical state. The aperture on the critical state line (*CSL*) is given as

$$b = b_s - \lambda ln\frac{\sigma_n}{p_a} \tag{10}$$

where b_s is the aperture on the critical state line at $\sigma_n = P_a$.

In this study, the cyclic loading and unloading tests were conducted before the shear process. The influence of the stress history was considered in the modeling. Barton [4] claimed that the influence of the stress history on the rock joints is similar to that on the soil. The terminology "over-closed" was proposed to distinguish the normally-loaded and the pre-loaded joints, which, in concept, is close to the over-consolidated state of soil material [1, 10, 14, 31]. Here, after the cyclic loading/unloading process, the rock joint is defined at the over-closed state. Under the constant normal load condition, it finally reaches the critical state after the shear process. The aperture variation is shown in **Fig. 8**.

Aperture b_{sbs} on the state boundary surface can be obtained by

$$b_{sbs} = b_n - (b_n - b_s)\zeta(\eta) - \lambda ln\frac{\sigma_n}{p_a} \tag{11}$$

where $\zeta(\eta)$ is an increasing function of the stress ratio. It satisfies $\zeta(0) = 0$ on the compression line and $\zeta(M) = 1$ on the *CSL*. In this study, the state function is defined as

$$\zeta(\eta) = \frac{\ln\left\{1 + \left(\frac{\eta}{M}\right)^2\right\}}{\ln 2} \tag{12}$$

In the present study, the subloading surface concept was adopted to describe the plastic closure induced by the stress inside the yield surface. It is an unconventional elastoplastic model that satisfies the mechanical requirements involving the continuity condition and the smoothness condition [28]. State parameter Ω is introduced to describe the distance between the current state and the state boundary surface. Based on this concept, the stress inside the yield surface can smoothly approach the state boundary surface. **Fig. 9** illustrates the modeling of the aperture with state parameter Ω. The distance of the current aperture from the state boundary surface is represented as

$$\Omega = b_{sbs} - b = b_n - (b_n - b_s)\zeta(\eta) - \lambda ln\frac{\sigma_n}{p_a} - b \tag{13}$$

Then, combining the subloading concept and the critical state, the arbitrary aperture is obtained by rewriting Eq. (13), as follows:

$$b = b_n - (b_n - b_s)\zeta(\eta) - \lambda ln\frac{\sigma_n}{p_a} - \Omega \tag{14}$$

The initial aperture, b_0, is calculated by inputting the initial normal stress as $\sigma_n = \sigma_{n0}$, the shear stress as $\sigma_s = 0$, and the stress ratio as $\eta = 0$ in Eq. (15).

$$b_0 = b_n - \lambda ln\frac{\sigma_{n0}}{p_a} - \Omega_0 \tag{15}$$

The increment of aperture, Δb, is the magnitude from the initial state to the current state. Δb can be calculated by substituting Eq. (14) into Eq. (15).

$$\Delta b = (b_n - b_s)\zeta(\eta) - \lambda ln\frac{\sigma_n}{\sigma_{n0}} + (\Omega - \Omega_0) \tag{16}$$

By substituting Eqs. (3), (10), and (16) into Eq. (2), plastic displacement deformation $\Delta\delta_n^p$ can be obtained.

$$\Delta\delta_n^p = (b_n - b_s)\zeta(\eta) + (\lambda - \kappa)ln\frac{\sigma_n}{\sigma_{n0}} + (\Omega - \Omega_0) \tag{17}$$

From Eq. (17), the yield function involves the variation of aperture and can be written as follows:

$$f = (b_n - b_s)\zeta(\eta) + (\lambda - \kappa)ln\frac{\sigma_n}{\sigma_{n0}} + (\Omega - \Omega_0) - \delta_n^p \tag{18}$$

In the condition of $\mathrm{d}\delta_n^p = 0$, from Eq. (17), the evolution of Ω can be given as

$$d\Omega = -(b_n - b_s)\zeta(\eta) - (\lambda - \kappa)ln\frac{d\sigma_n}{\sigma_n} \tag{19}$$

or for $\mathrm{d}\delta_n^p \neq 0$, Ω gradually reaches zero with the plastic movement.

$$d\Omega = -R(\Omega)|d\boldsymbol{\delta^p}| \tag{20}$$

where $R(\Omega)$ is a function of Ω. Parameter ω is introduced to describe the rate of plastic strain approaching the normal yield surface.

$$R(\Omega) = \omega\Omega^2 \tag{21}$$

3.3 Associated flow rule

The associated flow rule is adopted in the proposed model for simplicity. Potential plastic function g is assumed to equal yield function *f*. The increment in plastic displacement is calculated by

297 $$d\delta^p = d\Lambda \frac{\partial f}{\partial \boldsymbol{\sigma}} \tag{22}$$

298 $$\begin{pmatrix} \mathrm{d}\delta_n^p \\ \mathrm{d}\delta_s^p \end{pmatrix} = d\Lambda \begin{pmatrix} \dfrac{\partial f}{\partial \sigma_n} \\ \dfrac{\partial f}{\partial \sigma_s} \end{pmatrix} \tag{23}$$

299 where $d\Lambda$ is a plastic multiplier.

300 At the critical state $(\eta = M)$ and under the continuous loading condition $(d\Lambda > 0)$, the

301 increment in relative plastic displacement is $d\delta_n^p = 0$. Then, b_s can be calculated by

302 $$b_s = b_n - ln2(\lambda - \kappa) \tag{24}$$

3.4 Elastoplastic stress-relative displacement relationship

303 During elastoplastic displacement deformation, the stress stays on the yield surface, and

304 the yield function is equal to zero. The consistency condition is satisfied as

305 $$df = \frac{\partial f}{\partial \boldsymbol{\sigma}} d\boldsymbol{\sigma} + \frac{\partial f}{\partial \delta_n^p} d\delta_n^p + \frac{\partial f}{\partial \Omega} d\Omega = 0 \tag{25}$$

306 Substituting Eqs. (2), (4), (20), and (21) into Eq. (23), the plastic multiplier is calculated as

307 $$d\Lambda = \frac{\dfrac{\partial f}{\partial \boldsymbol{\sigma}} \cdot \boldsymbol{D^e} : d\boldsymbol{\delta}}{\dfrac{\partial f}{\partial \sigma_n} + \dfrac{\partial f}{\partial \boldsymbol{\sigma}} : \boldsymbol{D^e} : \dfrac{\partial f}{\partial \boldsymbol{\sigma}} + R(\Omega) \left| \dfrac{\partial f}{\partial \boldsymbol{\sigma}} \right|} \tag{26}$$

308 The elastic relationship is given by incorporating Eq. (22).

309 $$d\boldsymbol{\sigma} = \boldsymbol{D^e} : (d\boldsymbol{\delta} - d\boldsymbol{\delta^p}) = \boldsymbol{D^e} : (d\boldsymbol{\delta} - d\Lambda \frac{df}{d\boldsymbol{\sigma}}) \tag{27}$$

310 Then, the elastoplastic stress-strain relationship can be expressed as

311 $$d\boldsymbol{\sigma} = \left[\boldsymbol{D^e} - \frac{\boldsymbol{D^e} : \dfrac{\partial f}{\partial \boldsymbol{\sigma}} \otimes \dfrac{\partial f}{\partial \boldsymbol{\sigma}} : \boldsymbol{D^e}}{\dfrac{\partial f}{\partial \sigma_n} + \dfrac{\partial f}{\partial \boldsymbol{\sigma}} : \boldsymbol{D^e} : \dfrac{\partial f}{\partial \boldsymbol{\sigma}} + R(\Omega) \left\| \dfrac{\partial f}{\partial \boldsymbol{\sigma}} \right\|} \right] \cdot d\boldsymbol{\delta} \tag{28}$$

312 Here, $\boldsymbol{D^{ep}}$ is the elastoplastic stiffness tensor.

313 $$\boldsymbol{D^{ep}} = \boldsymbol{D^{e}} - \frac{\boldsymbol{D^{e}}:\frac{\partial f}{\partial \boldsymbol{\sigma}} \otimes \frac{\partial f}{\partial \boldsymbol{\sigma}}:\boldsymbol{D^{e}}}{\frac{\partial f}{\partial \sigma_n} + \frac{\partial f}{\partial \boldsymbol{\sigma}}:\boldsymbol{D^{e}}:\frac{\partial f}{\partial \boldsymbol{\sigma}} + R(\Omega)\left\|\frac{\partial f}{\partial \boldsymbol{\sigma}}\right\|} \quad (29)$$

314 The effect of changing the aperture on the shearing behavior of joints is taken into account
315 properly. An elastoplastic model is proposed for the interface between intact rock masses. In
316 addition, a unified description of the stiffness, strength, and dilation characteristics can be
317 achieved by applying the modified critical state theory. The model can be easily implemented
318 to joint/interface elements in the FEM or FDM [32, 33]. Thus, the application of the model to
319 practical issues is relatively easy.

3.5 Determination of constitutive parameters

320 Use of the constitutive model reported in this paper requires the specifications of the
321 compression indexes, initial apertures, and critical state stress ratio. The constitutive parameters
322 (λ, κ, and b_0) can be determined by cyclic loading and unloading tests. Loading compression
323 index λ and unloading compression index κ are the slope of the first loading line and the
324 slope of the first unloading line in the semi-logarithmic plot, respectively. Initial aperture b_0
325 can be measured from the third unloading process by subtracting the normal closure from the
326 maximum closure. Critical state stress ratio M can be calibrated from the results of the direct
327 shear tests.

328 Parameter b_n is the average aperture under atmospheric pressure that corresponds to the
329 theoretical maximum value of the average aperture. This parameter is obtained from a backward

analysis. The value is assumed to equal the calibrated results for the aperture at the residual state. The rest of the parameters (α, μ, and ω), which control the deformation of the horizontal and vertical directions, and the rate of plastic strain, can be obtained by fitting the results of a numerically simulated test to the results of the direct shear experiment.

4 Model prediction

To validate the capability of the proposed model, the shear behavior of discontinuous rock masses was analyzed. Comparisons were made between the numerical simulation responses and the experimental results from the direct shear tests. The cases under consideration include the first shear process and the second shear process of the four granite specimens, which have different initial apertures, uniaxial compressive strength, and confining pressure.

4.1 Direct shear tests on discontinuous rock masses

The fresh joint before the shear process is seen to have a relatively smaller initial aperture than afterwards, since the upper and lower joint surfaces of the specimen match well. The first shear process was conducted on four jointed granite specimens to check the numerical simulation result. The constitutive parameters are shown in **Table 3**. **Fig. 10** presents a comparison between the first shear experimental and numerical simulation results for the four granite specimens. The comparison results demonstrated that the numerical simulation results have an excellent agreement with the experimental results for the four fresh rock joints with different initial apertures. It was confirmed that the proposed model is able to capture the

softening tendency of the shear process and the tendency of dilatancy in the discontinuous rock mass. The peak and residual shear stress can be predicted by the proposed model. Moreover, a good concordance can be observed between the experimental and numerical curves of dilation. For the fresh specimens, the peak strength in the experimental results occurs later or earlier than in the analytical prediction. These observations suggest that the fresh upper and lower surfaces need a small horizontal displacement to be tightly contacted and perfectly matched. The inaccuracies in the peak shear displacement between the experiment and the analysis stem from the initial contact condition in the shear box. The deviated displacement principally depends on the conditions of the experimental set-up.

The second shear process conducted on the four jointed granite specimens was also utilized to validate the proposed model. The constitutive parameters are shown in **Table 4**. After the first shear process, the breaking of the asperity creates a loosely matched joint and then causes an enlargement of the initial aperture. The initial apertures of the four sheared specimens increased to a certain extent more than the initial apertures of the fresh samples, respectively. Moreover, the loading/unloading compression indices also increased after the shear process. **Fig. 11** shows a comparison between the experimental and numerical simulation results of the second shear process for the four sheared specimens. The constitutive model shows a good agreement with the evolution of the dilation during the shear process. Moreover, the constitutive model can capture the hardening tendency of the sheared rock joints. The peak strength is

366 reasonably well predicted by the model, although specimen G2 of the second shear process still
367 shows large peak strength in the initial shear phase. This peak strength is attributed to the
368 presence of the remaining rough asperity on the interfaces, which is not taken into account in
369 the proposed model.

370 Overall, the softening and hardening behavior in the first and second shear processes was
371 properly described by the proposed model, respectively. The aperture dilation was also well
372 captured during the two shear processes. Moreover, the relationship between the initial aperture
373 and the shear strength and dilation was confirmed by the analysis model. The smaller initial
374 aperture in the fresh rock joints tends to cause the apparent peak shear strength and larger
375 dilation. Conversely, the larger initial aperture in the sheared rock joints demonstrates the non-
376 salient peak shear strength and smaller dilation. The influence of the initial aperture on the
377 mechanical behavior is discussed in the following section.

4.2 Parametric study via the proposed model

378 The influence of the initial aperture on the numerical shear response was investigated by
379 applying the developed model. The constitutive parameters for specimen G1 in Case-1 and the
380 same constant confining stress were employed to simulate the shear stress, the normal
381 displacement, and the aperture dilation during the shear process. The analysis was performed
382 with different initial apertures ranging from 0.01 mm to 0.12 mm. **Fig. 12** shows the effect of
383 the different initial apertures on the shear behavior of specimen G1.

From **Figs. 12 (a) and (b)**, it is observed that the initial aperture significantly affects the shear stress and the normal displacement in the numerical simulation. As with the initial aperture increasing, both the peak shear stress and the dilation of the normal displacement decrease during the shear process. Namely, the smaller initial aperture corresponds to the higher peak shear strength and the more significant dilation. This tendency coincides with the present experimental results in the first and second shear process. Meanwhile, the responses whereby the open rock joints have lower frictional resistance and small dilation than the closed rock joints were also confirmed by the previous study [13, 34]. **Fig. 12 (c)** presents the aperture evolution, with different initial values, predicted by the proposed model. In contrast with the larger initial aperture, the smaller aperture must deform greatly to reach the final aperture state.

5 Conclusion

This study highlighted the variation and the effect of the joint aperture in cyclic compression tests and repeated shear tests. An elastoplastic model was proposed for rock joints incorporating the critical state concept and the aperture variation.

The model performance was validated by predicting the experimental results of rock joints. The hardening and softening shear behavior in the first and second shear processes was successfully described by the proposed model. Moreover, the dilation behavior in the fresh and sheared rock joints was also replicated during the two shear processes. The parameter study showed that the initial aperture controls the peak shear strength and dilation of rock joints. It

was seen that a rock joint mass with a small initial aperture tends to cause the apparent peak shear stress, while a rock joint mass with a larger initial aperture usually reaches the final shear state without salient peak shear stress. In addition, it was found that a small initial aperture usually responds to the great normal displacement during the shear process.

The proposed model is an elastoplastic model for the interface between intact rock masses. A unified description of the stiffness, strength, and dilation characteristics can be achieved by applying the modified critical state theory. Thus, the developed model can be readily employed in the analysis methods by incorporating the joint aperture.

Acknowledgements

The first author extends his appreciation for the financial support of the Japanese Government (MEXT) Scholarship and the Chinese Scholarship Council.

References

[1] Barton N. Review of a new shear-strength criterion for rock joints. Eng Geol 1973; 7:287–332. https://doi.org/10.1016/0013-7952(73)90013-6.

[2] Kulhawy FH. Stress deformation properties of rock and rock discontinuities. Eng Geol 1975; 9:327–50. https://doi.org/10.1016/0013-7952(75)90014-9.

[3] Zhao J. Joint surface matching and shear strength. Part A: joint matching coefficient (JMC). Int J Rock Mech Min Sci 1997; 34:173–8. https://doi.org/10.1016/S0148-9062(96)00062-9.

[4] Grasselli G, Egger P. Constitutive law for the shear strength of rock joints based on three-dimensional

surface parameters. Int J Rock Mech Min Sci 2003; 40:25–40. https://doi.org/10.1016/S1365-1609(02)00101-6.

[5] Xia CC, Yue ZQ, Tham LG, Lee CF, Sun ZQ. Quantifying topography and closure deformation of rock joints. Int J Rock Mech Min Sci 2003; 40:197–220. https://doi.org/10.1016/S1365-1609(02)00134-X.

[6] Li Y, Oh J, Mitra R, Hebblewhite B. A constitutive model for a laboratory rock joint with multi-scale asperity degradation. Comput Geotech 2016; 72:143–51. https://doi.org/10.1016/j.compgeo.2015.10.008.

[7] Plesha ME. Constitutive models for rock discontinuities with dilatancy and surface degradation. Int J Numer Anal Methods Geomech 1987; 11:345–62. https://doi.org/10.1002/nag.1610110404.

[8] Lee HS, Park YJ, Cho TF, You KH. Influence of asperity degradation on the mechanical behavior of rough rock joints under cyclic shear loading. Int J Rock Mech Min Sci 2001; 38:967–80. https://doi.org/10.1016/S1365-1609(01)00060-0.

[9] Kikumoto M, Nguyen VPQ, Yasuhara H, Kishida K. Constitutive model for soft rocks considering structural healing and decay. Comput Geotech 2017; 91:93–103. https://doi.org/10.1016/j.compgeo.2017.07.003.

[10] Kang X, Liao H. Bounding surface plasticity model for jointed soft rocks considering overconsolidation and structural decay. Comput Geotech 2019; 108:295–307. https://doi.org/10.1016/j.compgeo.2018.12.029.

[11] Kang X, Liao H. A bounding surface plasticity model consideringspacing ratio for overconsolidated jointed soft rocks. Rock Mech Rock Eng 2020; 53:59–69. https://doi.org/10.1007/s00603-019-01883-9.

[12] Tang ZC, Liu QS, Xia CC, Song YL, Huang JH, Wang CB. Mechanical model for predicting closure behavior of rock joints under normal stress. Rock Mech Rock Eng 2013; 47:2287–98. https://doi.org/10.1007/s00603-013-0499-z.

[13] Li Y, Oh J, Mitra R, Hebblewhite B. Experimental studies on the mechanical behaviour of rock joints with various openings. Rock Mech Rock Eng 2016; 49:837–53. https://doi.org/10.1007/s00603-015-0781-3.

[14] Barton N, Bandis S, Bakhtar K. Strength, deformation and conductivity coupling of rock joints. Int J Rock Mech Min Sci Geomech Abstr 1985; 22:121–40. https://doi.org/10.1016/0148-9062(85)93227-9.

[15] Bandis SC. Fundamentals of Rock Joint Deformation. Int J Rock Mech Min Sci 1983; 20:249–68. https://doi.org/10.1016/0148-9062(83)90595-8

[16] King MS. Wave velocities in rocks as a function and pore fluid of changes in overburden. Geophyscs 1966; 16:50–73. https://doi.org/10.1190/1.1439763

[17] Gordon RB, Davis LA. Velocity and attenuation of seismic waves in imperfectly elastic rock. J Geophys Res 1968; 73:3917–35. https://doi.org/10.1029/jb073i012p03917.

[18] Pyrak-Nolte LJ, Myer LR, Cook NGW, Witherspoon PA. Hydraulic and mechanical properties of natural fractures in low permeability rock. 6th Int. Congr. Rock Mech., 1987, p. 224–31.

[19] Hopkins DL. The implications of joint deformation in analyzing the properties and behavior of fractured rock masses, underground excavations, and faults. Int J Rock Mech Min Sci 2000; 37:175–202. https://doi.org/10.1016/s1365-1609(99)00100-8.

[20] Malama B, Kulatilake PHSW. Models for normal fracture deformation under compressive loading. Int J

Rock Mech Min Sci 2003; 40:893–901. https://doi.org/10.1016/S1365-1609(03)00071-6.

[21] Esaki T, Du S, Mitani Y, Ikusada K, Jing L. Development of a shear-flow test apparatus and determination of coupled properties for a single rock joint. Int J Rock Mech Min Sci 1999; 36:641–50. https://doi.org/10.1016/S0148-9062(99)00044-3.

[22] Matsuki K, Chida Y, Sakaguchi K, Glover PWJ. Size effect on aperture and permeability of a fracture as estimated in large synthetic fractures. Int J Rock Mech Min Sci 2006; 43:726–55. https://doi.org/10.1016/j.ijrmms.2005.12.001.

[23] Sharifzadeh M, Mitani Y, Esaki T. Rock joint surfaces measurement and analysis of aperture distribution under different normal and shear loading using GIS. Rock Mech Rock Eng 2008; 41:299–323. https://doi.org/10.1007/s00603-006-0115-6.

[24] Koyama T, Li B, Jiang Y, Jing L. Numerical modelling of fluid flow tests in a rock fracture with a special algorithm for contact areas. Comput Geotech 2009; 36:291–303. https://doi.org/10.1016/j.compgeo.2008.02.010.

[25] Samuelson J, Elsworth D, Marone C. Shear-induced dilatancy of fluid-saturated faults: Experiment and theory. J Geophys Res Solid Earth 2009; 114:1–15. https://doi.org/10.1029/2008JB006273.

[26] Roscoe KH, Schofield AN, Thurairajah A. Yielding of clays in states wetter than critical. Géotechnique 1963; 13:211–40. https://doi.org/10.1680/geot.1963.13.3.211.

[27] Schofield A, Wroth P. Critical state soil mechanics. vol. 310. McGraw-Hill, London;1968.

[28] Hashiguchi K. Foundations of elastoplasticity: subloading surface model. Cham: Springer International

476 Publishing; 2017. https://doi.org/10.1007/978-3-319-48821-9.

477 [29] Goodman RE. The mechanical properties of joints. Proc 3rd Congr ISRM, Denver, 1974; 1A:127–40.

478 [30] Saeb S, Amadei B. Modelling Rock Joints under Shear and Normal Loading. Int J Rock Mech Min Sci

479 Geomech Abstr 1992; 29:267–78. https://doi.org/10.1016/0148-9062(92)93660-C.

480 [31] Zhu H, Ye B, Cai Y, Zhang F. An elasto-viscoplastic model for soft rock around tunnels considering

481 overconsolidation and structure effects. Comput Geotech 2013; 50:6–16.

482 https://doi.org/10.1016/j.compgeo.2012.12.004.

483 [32] Bfer G. An isoparametric joint/interface element for finite element analysis. Int J Numer Methods Eng

484 1985; 21:585–600. https://doi.org/10.1002/nme.1620210402.

485 [33] Gens A, Carol I, Alonso EE. Rock joints: FEM implementation and applications. Stud. Appl. Mech., vol.

486 42, 1995, p. 395–420. https://doi.org/10.1016/S0922-5382(06)80019-X.

487 [34] Oh J, Kim GW. Effect of opening on the shear behavior of a rock joint. Bull Eng Geol Environ 2010;

488 69:389–95. https://doi.org/10.1007/s10064-010-0271-5.

489 [35] Kishida K, Kawaguchi Y, Nakashima S, Yasuhara H. Estimation of shear strength recovery and

490 permeability of single rock fractures in shear-hold-shear type direct shear tests. Int J Rock Mech Min Sci

491 2011; 48:782–93. https://doi.org/10.1016/j.ijrmms.2011.04.002.

492

List of symbols

σ_n, σ_{n0} normal stress and initial normal stress

v_j closure of joint aperture

V_{mc} maximum closure of joint aperture

$\boldsymbol{\delta}$ total relative displacement

$\boldsymbol{\sigma}$ traction vector

$\boldsymbol{\delta^e}$, $\boldsymbol{\delta^p}$ elastic and plastic components of total relative displacement

δ_n, δ_s normal relative displacement and shear relative displacement

δ_n^e, δ_s^e elastic component of normal and shear relative displacement

δ_n^p, δ_s^p plastic component of normal and shear relative displacement

λ, κ loading compression index and unloading compression index

k_n, k_s normal stiffness and shear stiffness

k_{ns} stiffness controlling effect of shearing on confining stress

$\boldsymbol{D^e}$, $\boldsymbol{D^{ep}}$ elastic stiffness tensor and elastoplastic stiffness tensor

μ, α constant coefficients

b, Δb joint aperture and joint aperture variation

b_n, b_s joint aperture on first normal loading line and critical state line under atmospheric pressure

b_{sbs} joint aperture on state boundary surface

η, $\zeta(\eta)$ stress ratio and function of stress ratio

M critical state stress ratio

Ω, $R(\Omega)$ distance of current joint aperture from state boundary surface and function of Ω

ω rate of plastic strain approaching normal yield surface

f, g yield function and potential plastic function

$d\Lambda$ plastic multiplier

Tables and Figures

517

518 **Tables**

523

524 **Figures**

544

Table 1 Mechanical properties of granite specimens

Specimen No.	Uniaxial compressive strength [MPa]	Basic friction angle [°]	Normal stiffness [MPa/mm]
G1	140.31	38.8	60.85
G2	140.31	38.8	60.85
G3	80.5	42.3	2.673
G4	80.5	42.3	2.673

Table 2 Experimental conditions

Specimen No.	Case No.	Compression test Loading stress (σ_n, MPa)	Shear test Loading stress (σ_n, MPa)	Joint roughness coefficient (JRC)	Initial joint aperture (b_0, mm)
G1	Case-1	0.5-3.0	3.0	13.45	0.0285
	Case-2	0.3-3.0	3.0	3.84	0.0449
G2	Case-1	0.3-3.0	3.0	16.15	0.0043
	Case-2	0.3-3.0	3.0	8.53	0.0654
G3	Case-1	0.1-1.0	1.0	20.93	0.0147
	Case-2	0.1-1.0	1.0	9.74	0.0283
G4	Case-1	0.1-1.0	1.0	18.81	0.0243
	Case-2	0.1-1.0	1.0	8.50	0.0451

570 **Table 3** Constitutive parameters for rock joint before shear process

Index	Parameter	G-1	G-2	G-3	G-4
λ	Loading compression index	0.0191	0.0320	0.0423	0.0560
κ	Unloading compression index	0.0021	0.0069	0.0302	0.0355
M	Critical state stress ratio	0.9459	0.9459	0.9099	0.9099
b_n	Average aperture under atmospheric pressure	1.2	1.2	1.2	1.2
b_0	Initial aperture	0.0285	0.0043	0.0147	0.0243
μ	Ratio between k_s and k_n	1	1	1	1
α	Ratio between k_{ns} and k_n	0.1	0.3	0.3	0.3
ω	Rate of the evolution	0.85	1.40	0.85	0.80

571

572 **Table 4** Constitutive parameters for rock joint after shear process

Index	Parameter	G-1	G-2	G-3	G-4
λ	Loading compression index	0.0703	0.1806	0.0763	0.0969
κ	Unloading compression index	0.0216	0.0868	0.0691	0.0895
M	Critical state stress ratio	0.9459	0.9459	0.9099	0.9099
b_n	Average aperture under atmospheric pressure	1.2	1.2	1.2	1.2
b_0	Initial aperture	0.0449	0.0654	0.0283	0.0451
μ	Ratio between k_s and k_n	1	1	1	1
α	Ratio between k_{ns} and k_n	0.2	0.5	0.2	0.2
ω	Rate of the evolution	0.01	0.60	0.10	0.10

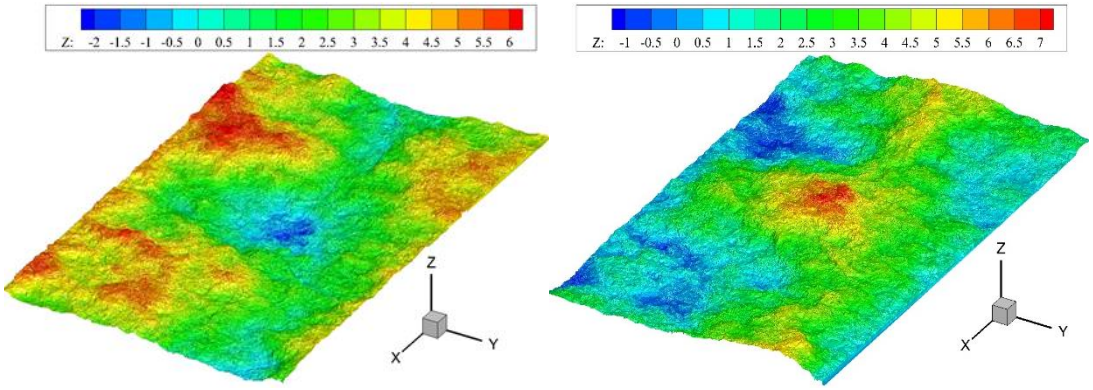

(a) Lower surface of G1 (b) Upper surface of G1

Fig. 1 Contour map of joint surface roughness of specimen G1: (a) Lower surface of G1 and (b) Upper surface of G1

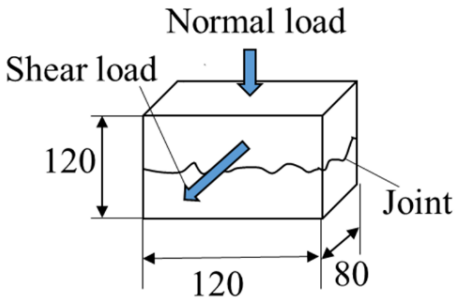

(a)

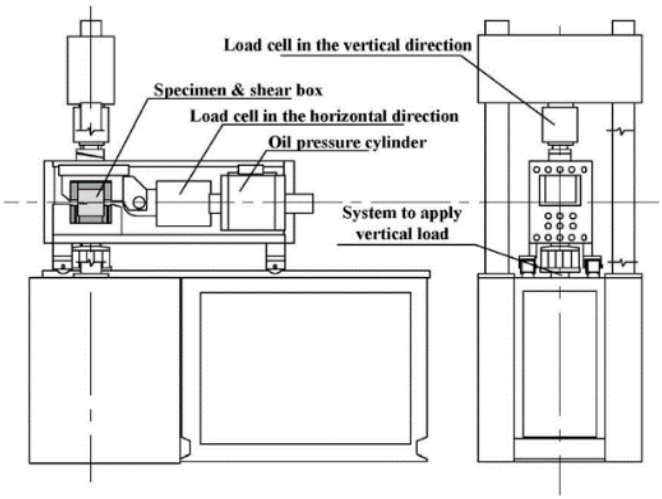

(b)

Fig. 2 Outlines of rock sample and apparatus: (a) Rock sample with single joint and (b) Apparatus including compression and shear unit [35]

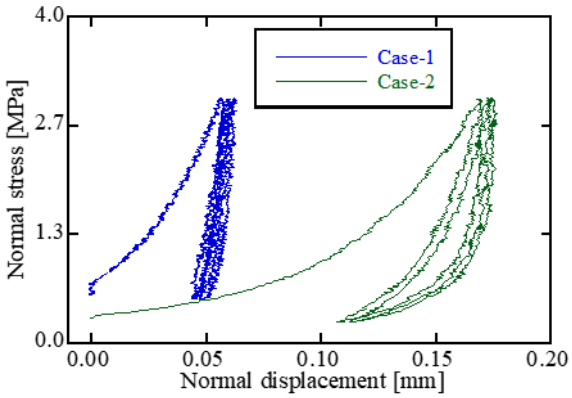

(a)

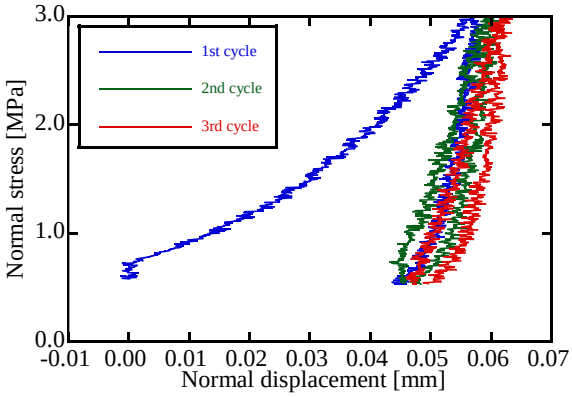

(b)

Fig. 3 Normal displacement-stress relation of cyclic loading and unloading tests in granite specimen G1: (a) Overview and (b) Enlarged view of Case-1

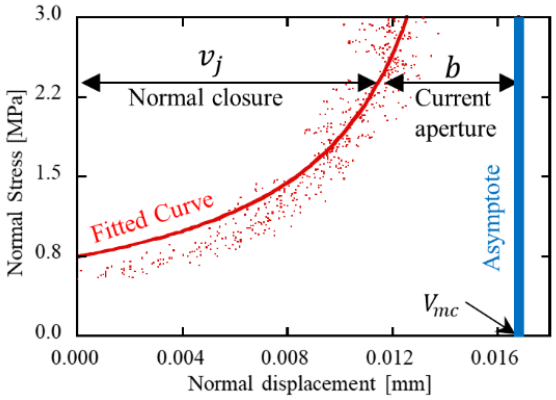

598

599

600 **Fig. 4** Fitted hyperbolic curve of third unloading path of Case-1 in specimen G1

601

602

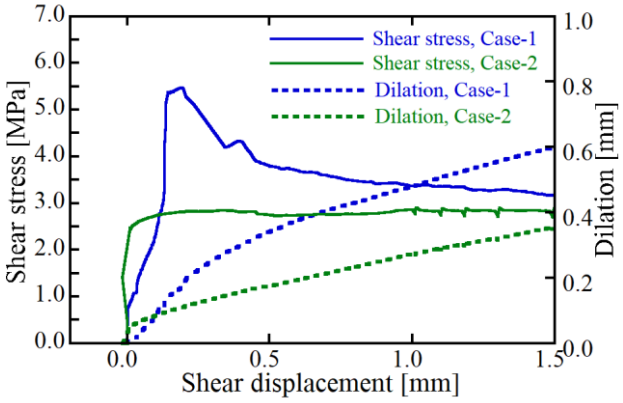

603

604 (a)

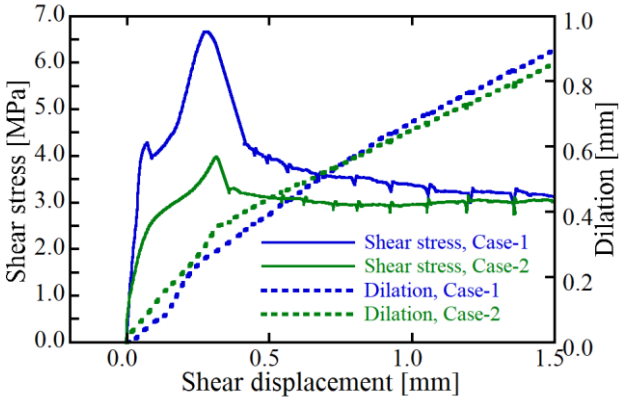

605

606 (b)

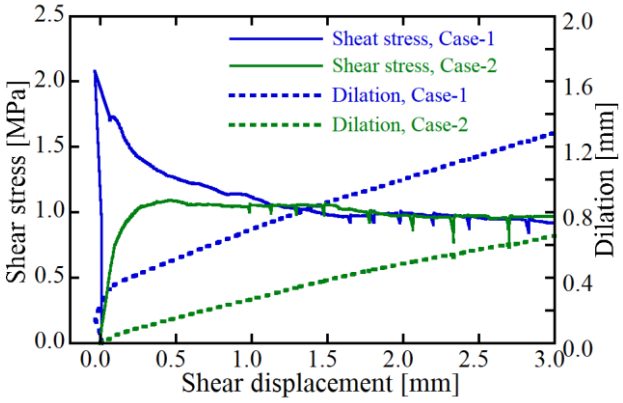

(c)

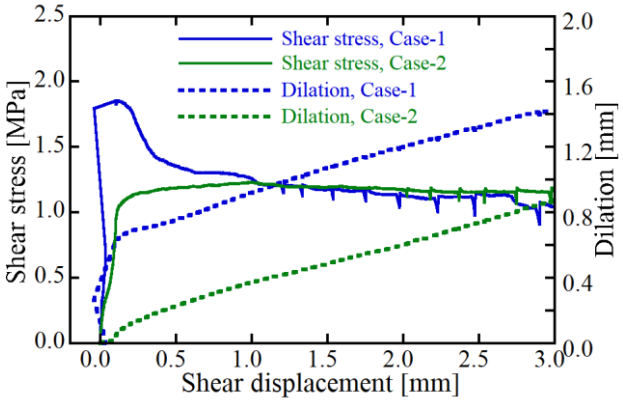

(d)

Fig. 5 Shear displacement-stress relationship of two cases in four granite specimens: (a) Case-1 and (b) Case-2

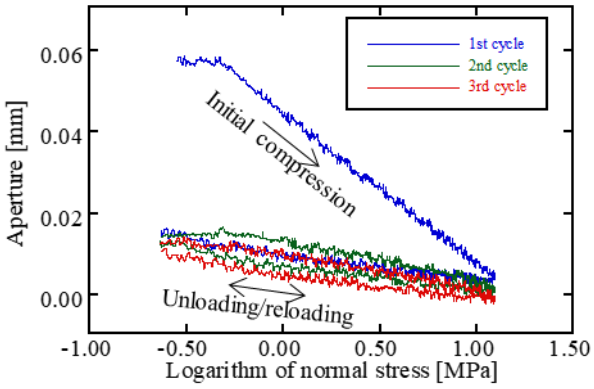

Fig. 6 Aperture evolution during compression tests of Case-1 in specimen G1

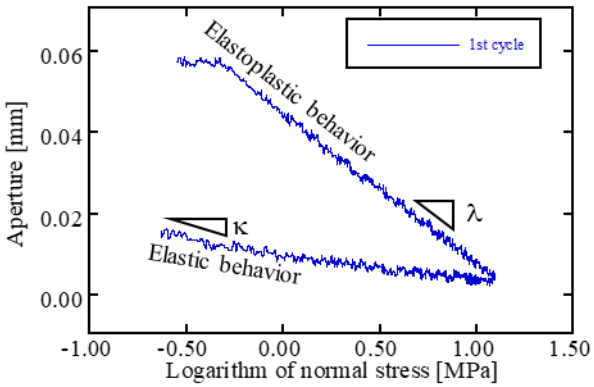

615

616 **Fig. 7** Typical deformation behavior of Case-1 in specimen G1

617

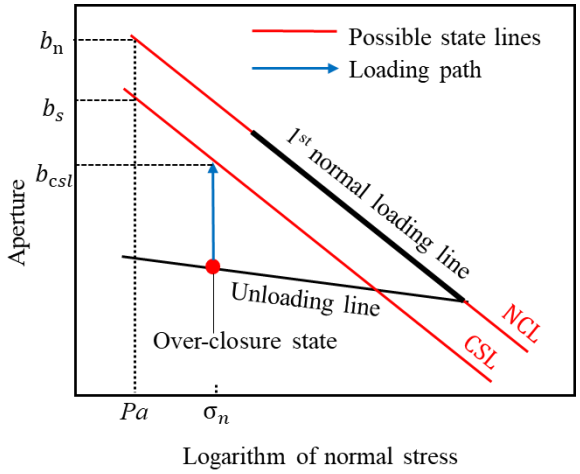

618

619 **Fig. 8** Modeling of aperture in rock joint

620

621

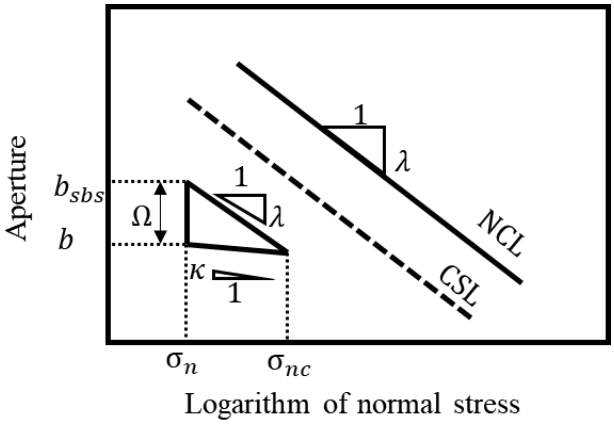

622

623 **Fig. 9** Modeling of aperture in rock joint with state parameter Ω

624

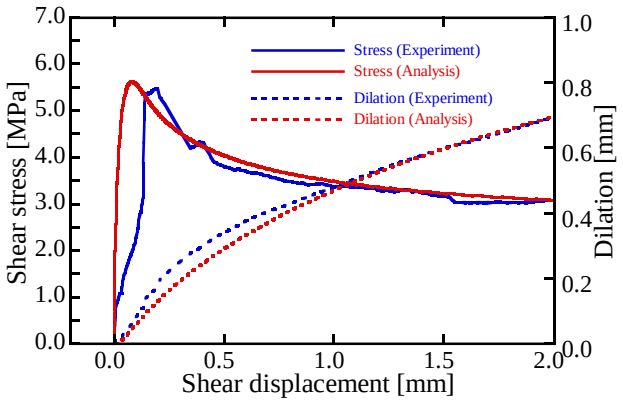
Stress (Experiment)
Stress (Analysis)
Dilation (Experiment)
Dilation (Analysis)
Shear stress [MPa]
Dilation [mm]
Shear displacement [mm]
0.0
1.0
2.0
3.0
4.0
5.0
6.0
7.0
0.2
0.4
0.6
0.8
0.5
1.5

(a)

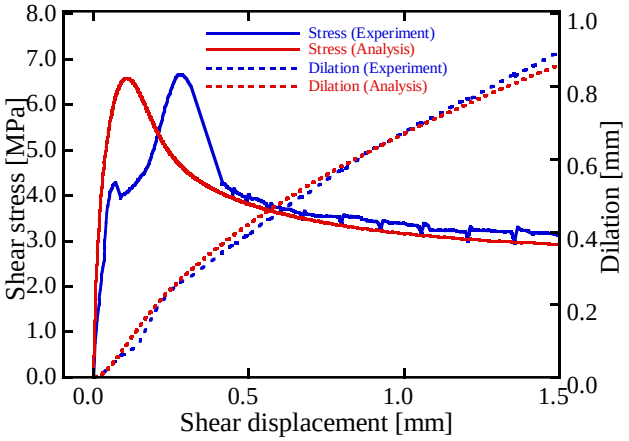
Stress (Experiment)
Stress (Analysis)
Dilation (Experiment)
Dilation (Analysis)
Shear stress [MPa]
Dilation [mm]
Shear displacement [mm]
0.0
1.0
2.0
3.0
4.0
5.0
6.0
7.0
8.0
0.2
0.4
0.6
0.8
0.5
1.5

(b)

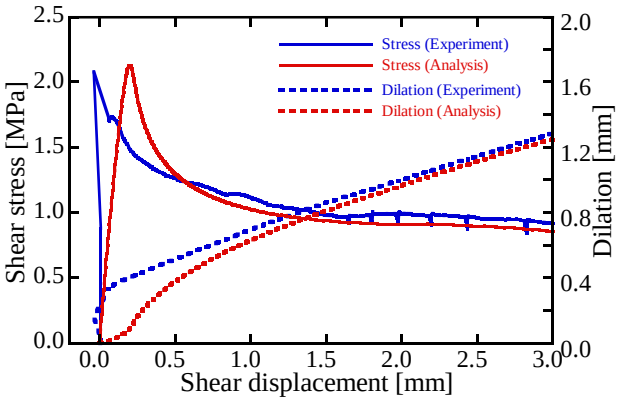
Stress (Experiment)
Stress (Analysis)
Dilation (Experiment)
Dilation (Analysis)
Shear stress [MPa]
Dilation [mm]
Shear displacement [mm]
0.0
0.5
1.0
1.5
2.0
2.5
3.0
0.4
0.8
1.2
1.6

(c)

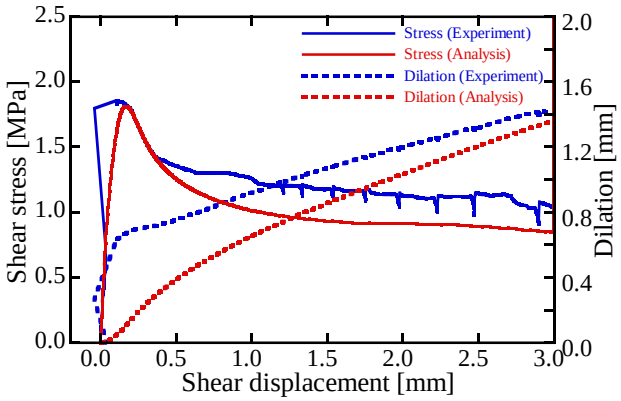

(d)

Fig. 10 Comparison of first shear experimental and numerical simulation results on four granite specimens: (a) Specimen G1 under confining stress of σ_n=3 MPa, (b) Specimen G2 under confining stress of σ_n=3 MPa, (c) Specimen G3 under confining stress of σ_n=1 MPa, and (d) Specimen G4 under confining stress of σ_n=1 MPa

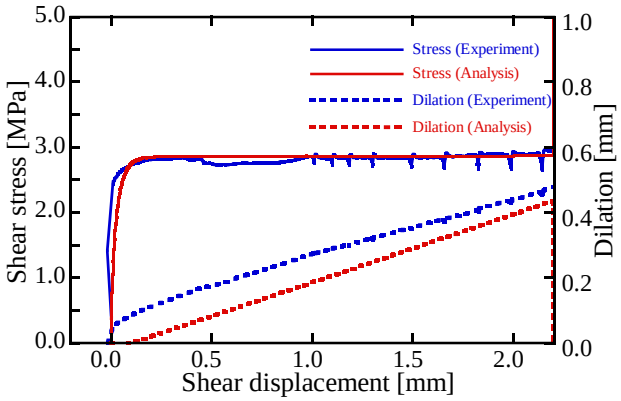

(a)

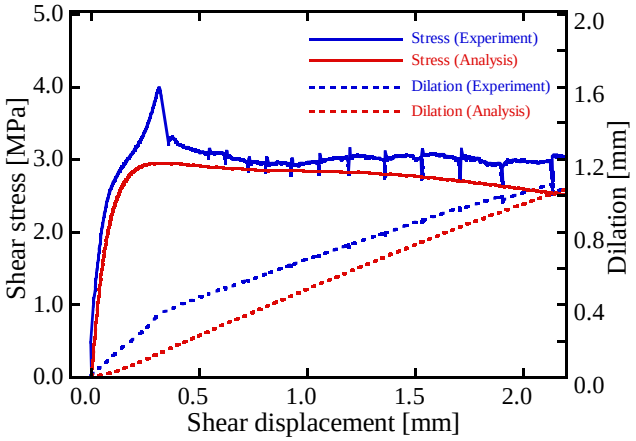

(b)

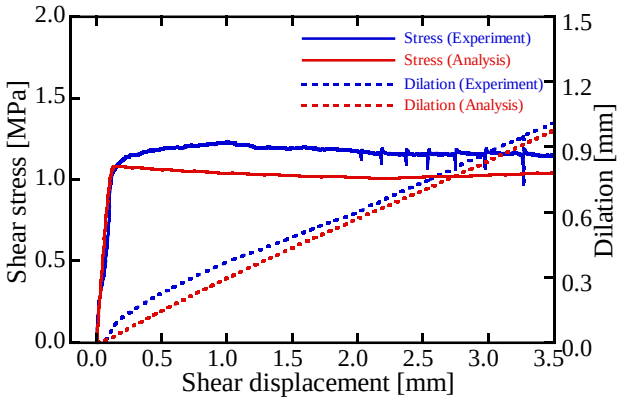

(c)

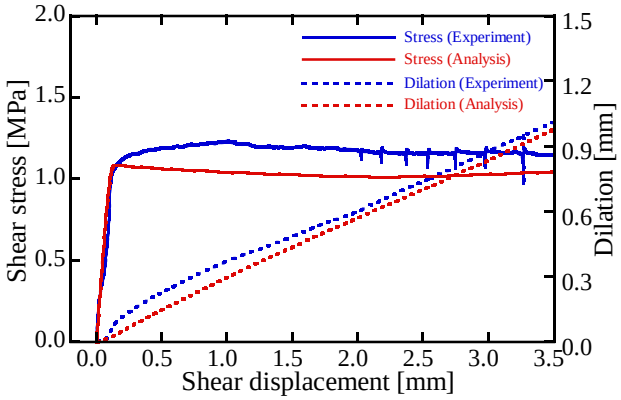

(d)

Fig. 11 Comparison of second shear experimental and numerical simulation results on four granite specimens: (a) Specimen G1 under confining stress of σ_n=3 MPa, (b) Specimen G2 under confining stress of σ_n=3 MPa, (c) Specimen G3 under confining stress of σ_n=1 MPa, and (d) Specimen G4 under confining stress of σ_n=1 MPa

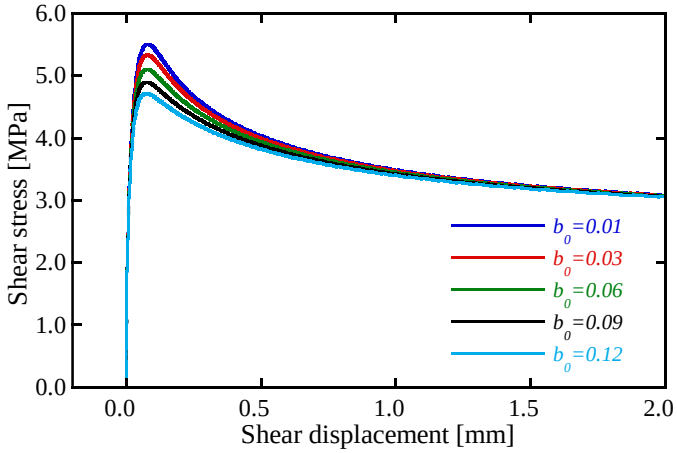

(a)

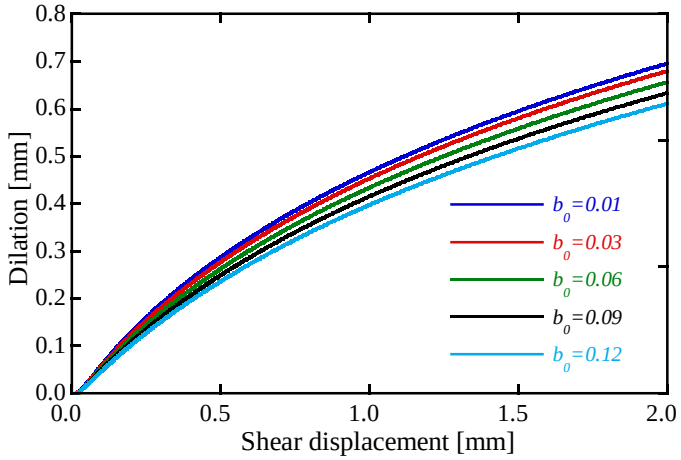

(b)

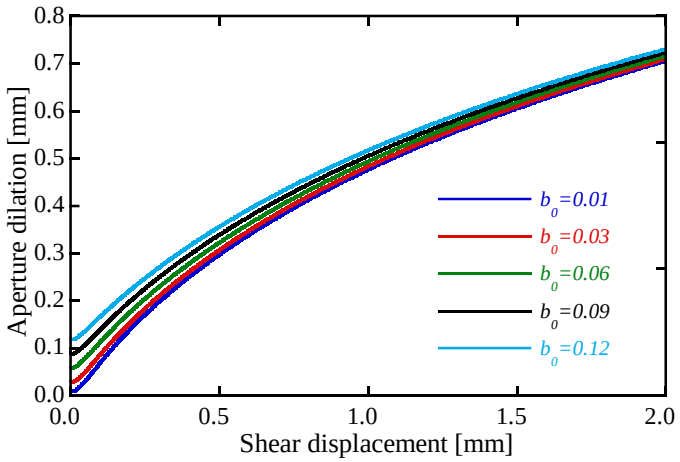

(c)

Fig. 12 Simulation results of effect of initial aperture on shear behavior: (a) Influence on shear strength, (b) Influence on normal displacement, and (c) Influence on aperture dilation